




OPEN

Human glioblastoma-derived cell membrane nanovesicles: a novel, cell-specific strategy for boron neutron capture therapy of brain tumors

Alice Balboni^{1,7}, Giorgia Ailuno^{1,7}✉, Sara Baldassari¹, Giuliana Drava¹, Andrea Petretto², Nicole Grinovero², Ornella Cavalleri³, Elena Angeli³, Andrea Lagomarsino³, Paolo Canepa³, Alessandro Corsaro⁴, Beatrice Tremonti⁴, Federica Barbieri⁴ , Stefano Thellung⁴, Paola Contini⁴, Katia Cortese⁵, Tullio Florio^{4,6,8}✉ & Gabriele Caviglioli^{1,6,8}

Glioblastoma (GBM), one of the deadliest brain tumors, accounts for approximately 50% of all primary malignant CNS tumors, therefore novel, highly effective remedies are urgently needed. Boron neutron capture therapy, which has recently repositioned as a promising strategy to treat high-grade gliomas, requires a conspicuous accumulation of boron atoms in the cancer cells. With the aim of selectively deliver sodium borocaptate (BSH, a 12 B atoms-including molecule already employed in the clinics) to GBM cells, we developed novel cell membrane-derived vesicles (CMVs), overcoming the limits of natural extracellular vesicles as drug carriers, while maintaining their inherent homing abilities that make them preferable to fully synthetic nanocarriers. Purified cell membrane fragments, isolated from patient-derived GBM stem-like cell cultures, were used to prepare nanosized CMVs, which retained some membrane proteins specific of the GBM parent cells and were devoid of potentially detrimental genetic material. In vitro tests evidenced the targeting ability of this novel nanosystem and ruled out any cytotoxicity. The CMVs were successfully loaded with BSH, by following two different procedures, i.e. sonication and electroporation, demonstrating their potential applicability in GBM therapy.

Keywords Cell membrane, Cancer treatment, Bioinspired vesicles, Cell internalization, Proteomics

Diffuse gliomas are the most prevalent malignant and deadliest primary brain tumors in adults¹. Glioblastoma IDH-wild type WHO 4 (GBM)², accounting for approximately 50% of all primary malignant CNS tumors³, presents very poor prognosis and a median survival of about 15 months⁴; it is characterized by uncontrolled cell proliferation, diffuse infiltration and necrosis, and robust angiogenesis⁵, which largely depend on the presence and activity of cancer stem cells within the tumor mass². Usually, GBM patients at diagnosis display non-specific neurological symptoms, like headaches, seizures, focal neurologic deficits, memory loss, visual changes, personality changes, and vomiting^{1,6}. Current standard treatment for GBM includes maximal surgical resection followed by concurrent radiotherapy with the alkylating drug temozolomide and further adjuvant temozolomide⁷. Although few new drugs have recently been approved for GBM treatment, the outcome is still largely unsatisfactory, and more effective therapies are urgently needed. Indeed, many innovative therapeutic approaches, involving combinations of radiotherapy with immunotherapy or nanoparticle (NPs)-vehiculated drugs, are currently under study⁸.

Exosomes, nanosized extracellular vesicles released by the majority of cell types, have been proposed as drug carriers due to their ability to shuttle biomolecules, their innate selectivity towards the parent cell of origin or cell

¹Department of Pharmacy, University of Genoa, 16148 Genoa, Italy. ²IRCCS Istituto Giannina Gaslini, 16147 Genoa, Italy. ³Department of Physics, University of Genoa, 16146 Genoa, Italy. ⁴Department of Internal Medicine, University of Genoa, 16132 Genoa, Italy. ⁵Department of Experimental Medicine, University of Genoa, 16132 Genoa, Italy. ⁶IRCCS Ospedale Policlinico San Martino, 16132 Genoa, Italy. ⁷These authors contributed equally: Alice Balboni and Giorgia Ailuno. ⁸These authors jointly supervised this work: Tullio Florio and Gabriele Caviglioli. ✉email: giorgia.ailuno@unige.it; tullio.florio@unige.it

type (i.e., homing ability), and their low immunogenicity⁹. However, exosome purification and characterization are challenging, and their yield and loading efficiency are relatively poor, limiting their large-scale application in the clinics¹⁰. Therefore, the generation of bioinspired exosome-mimetics with higher yield and consistency is attractive for drug delivery. Possible strategies to obtain exosome-mimetics are the isolation of cell membranes either directly used to manufacture cell-mimicking vesicles^{11,12} or employed for coating different kinds of NPs^{13,14}, or the formulation of hybrid vesicles fusing artificial liposomes and exosomes (or other types of cell-derived vesicles)¹⁵.

These innovative nanosystems might be suitable for vehiculating agents for Boron Neutron Capture Therapy (BNCT), a technique proposed as a treatment option for high-grade gliomas¹⁶, head and neck tumors^{17,18}, and cutaneous and extra-cutaneous melanomas^{19,20}. BNCT, involving the selective accumulation of chemical agents containing the ¹⁰B isotope in cancer cells, is based on capture and fission reactions occurring after irradiation with thermal neutrons: ¹⁰B neutron capture leads to the formation of excited ¹¹B, undergoing a nuclear fission response involving the emission of a high linear energy transfer α particle and a lithium nucleus. The short trajectory of the α particles allows to predominantly affect ¹⁰B-containing tumor cells, sparing more distant normal tissue, making BNCT suitable for circumscribed lesion treatment avoiding side effects typically associated with ionizing radiation²¹. The boron agents currently used in the clinics are boronophenylalanine (BPA) and sodium borocaptate (BSH). However, the limited tumor/normal tissue ratios of boron in patients treated with BSH and BPA promoted the development of more effective and selective boron delivery agents. In particular, boron-containing NPs are gaining increasing interest, and exosomes and biomimetic vesicles have also been studied as vehicles for BNCT agents²².

In the present paper, we describe the isolation of purified cell membrane fragments from patient-derived GBM stem-like cell cultures and their use to obtain cell membrane-derived nanovesicles (CMVs). Indeed, although several studies describe the use of GBM-derived cell membranes or GBM-derived exosomes to develop biomimetic nanosystems for drug delivery^{14,23–27}, to the best of our knowledge the development of vesicles composed of whole GBM cell membranes, like those we developed, have not been described in the literature yet; moreover, BSH encapsulation in biomimetic vesicles for BNCT of gliomas has not been reported either. The developed CMVs were characterized for their physical–chemical properties, morphology, and protein and genetic material content. BSH was loaded into CMVs by two different loading procedures, namely sonication and electroporation, and the cytocompatibility of the nanosystem with different types of cells was assessed. Then, internalization studies proved that the so-obtained CMVs featured targeting abilities towards the parent cells; moreover, CMVs exhibited high interaction also with non-parent GBM cells, with high specificity as compared to cultures of non-tumoral brain cells.

Materials and methods

Materials

BSH was purchased from Katchem; CellTracker™ CM-Dil red fluorescent dye and CellMask™ Green Plasma Membrane Stain from Thermo Fisher Scientific; Alexa Fluor® 488 Anti-Annexin-2/ANXA2 antibody [EPR13052(B)] from Abcam; analytical grade ethanol 96% and gradient grade methanol from VWR Chemicals. A starting buffer (225 mM mannitol, 75 mM sucrose and 30 mM Tris–HCl, pH 7.4) was used for CMVs preparation; the homogenizing buffer was obtained by adding 0.5% (w/v) BSA, 0.5 mM EGTA, 1 mM Na₃VO₄, and 1 mM PMFS to the starting buffer (all from Sigma-Aldrich).

Cell cultures

Human glioblastoma cultures (GBM1 and GBM2) were isolated from postsurgical specimens of patients who underwent surgery at IRCCS Ospedale Policlinico San Martino in Genoa, after informed consent and approval by the Institutional Ethical Committee (Comitato Etico Regione Liguria, register number CER Liguria, 360/2019). All methods were performed in accordance with relevant guidelines/regulations. Cells were grown in serum-free medium 1:1 DMEM-F12/Neurobasal™ (Gibco-Thermo Fisher Scientific) containing B27™ supplement (Gibco-Thermo Fisher Scientific), 2 mM L-glutamine (EuroClone), 1% penicillin–streptomycin (EuroClone), 15 µg/mL insulin and 2 µg/mL heparin (Sigma-Aldrich); 20 ng/mL human bFGF and 20 ng/mL EGF (Miltenyi Biotec) were added to enrich cultures in the stem-like population and allow the retainment of their biological features *in vitro*²⁸. Under these conditions, cells gave rise to floating tumor-spheres within 2 weeks, but to allow feasible and reliable experiments cells were grown as monolayers in flasks coated with growth factor-reduced Matrigel™ (Corning, Thermo Fisher Scientific), ensuring the maintenance of stem cell marker expression, spherogenic properties, differentiation and tumorigenic potential²⁹. Tumor-initiating activity was directly evaluated, in previous studies, by orthotopic xenografting in non-obese diabetic/severe combined immunodeficient mice³⁰. Human glial (oligodendrocytic) hybrid cell line M03.13 (Tebu-Bio) with phenotypic characteristics of normal primary oligodendrocytes (PubMed = 7707048; DOI = <https://doi.org/10.1002/neu.480260212>) was maintained in high glucose DMEM containing 10% FBS, 1% penicillin/streptomycin, 1% glutamine (all from Gibco, Thermo Fisher Scientific). M03.13 were differentiated in 100 nM phorbol 12-myristate 13-acetate (Sigma-Aldrich) and 1% FBS complete medium for five days prior to CMV treatment.

Preparation of cell homogenate

Human glioblastoma cells (GBM1), grown on Matrigel™ in 75 cm² culture flasks, were harvested with TryPLE (Thermo Fisher Scientific); 5 × 10⁸ cells were then homogenized on ice in homogenizing buffer at pH 7.4 using a Dounce glass homogenizer (100 strokes), to disrupt the whole cells but leaving intact the nuclei.

Preparation of CMVs

The homogenate from GBM1 underwent a differential centrifugation procedure, conducted in 1.5 mL Beckman centrifuge tubes at 4 °C. Firstly, the homogenate was centrifuged twice for 5 min at 800g; the supernatant was transferred in new tubes and centrifuged for 20 min at 10,000g. After collection, the supernatant was centrifuged for 20 min at 25,000g, then the supernatant was discarded and the pellet was washed twice with the starting buffer and twice with 0.9% NaCl, by centrifugating at 25,000g for 20 min. The obtained pellet, composed of cell membranes, was resuspended in 0.8 mL of mQ water or PBS buffer (pH 7.4), obtaining multilamellar CMVs, which were extruded through polycarbonate filters with decreasing pore size (400–200–100 nm, 20 passages for each filter) using an Avestin LiposoFast Basic semi-automatic extruder immersed in a water bath at 37 °C, with pressure set at 4 bar.

Some CMV batches were fluorescently labelled with CM-DiI solution in ethanol (2 pmol/μL). Prior to suspension in aqueous medium, the membrane pellet was added with an appropriate volume of CM-DiI solution, and the mixture was vortexed and sonicated until the pellet was suspended, then ethanol was gently evaporated under nitrogen flow at room temperature. After complete removal of the organic solvent, the pellet was resuspended in mQ water or PBS buffer (pH 7.4) and extruded as described above, obtaining red fluorescent labeled CMVs.

Preparation of BSH-loaded CMVs

To prepare BSH-loaded CMVs, two different loading methods were used: sonication and electroporation.

For the sonication-mediated loading, the cell membrane pellet obtained from the centrifugation procedure described in section “Preparation of CMVs” was hydrated with 0.6 mL of a 180 mM BSH aqueous solution, and the suspension was incubated under oscillation at 37 °C on a heating block for 30 min. Then, the suspension was extruded as previously reported and sonicated using a Branson 1510 Ultrasonic Cleaner for 6 cycles of 30 s on/off for 3 min with a 2 min cooling period between each cycle³¹. Then, the suspension was incubated under oscillation at 37 °C on a heating block for 1 h. The unencapsulated BSH was removed by washing and filtration using 100 kDa MWCO Amicon Ultra centrifugal filters.

For the electroporation procedure, 0.2 mL of CMV suspension in PBS mixed with an equal volume of a 180 mM BSH solution in PBS was electroporated in 0.4 mL electroporation cuvettes using an Eppendorf Multiporator[®] Electroporation Systems, with the following settings: two poring pulses of 100 V for 15 μs, followed by five transfer pulses of 20 V for 50 μs, with 1 min delay between each pulse. Then, the mixture was incubated under oscillation at 37 °C on a heating block for 1 h to ensure the CMV membrane fully recovered. Unencapsulated BSH was removed by washing and filtration using 100 kDa MWCO Amicon Ultra centrifugal filters. In both cases, before and after loading and purification, CMV mean size was measured, to detect any significant variation.

Characterization of CMVs

Size, zeta potential and concentration

Hydrodynamic diameter and zeta potential of extruded CMVs were measured, without further dilution, using a Malvern Zetasizer HSA 3000 equipped with a He/Ne lamp ($\lambda = 633$ nm). The average hydrodynamic diameter value was obtained from three measurements (10 sub runs each), with the software firstly acquiring the signal in non-negative least squares mode, then re-elaborating it through the CONTIN algorithm; the average zeta potential value was obtained from 5 measurements. CMV concentration was determined with a Malvern NanoSight NS300 equipped with a 532 nm laser, after diluting the CMV suspension 1:500 in mQ water.

Transmission electron microscopy (TEM)

CMV morphology was investigated using a Hitachi HT7800 transmission electron microscope equipped with a Megaview 3 digital camera and Radius software. CMVs were concentrated under N₂ flux for 2 h, then negative-staining was performed by adding 20 μL of 2% paraformaldehyde in 0.1 M phosphate buffer (pH 7.4) to 20 μL of CMV suspension in PBS (pH 7.2); the CMVs were then adsorbed for 20 min to formvar-carbon coated copper grids by floating the grids on 5 μL drops on parafilm. Subsequently, the grids were rinsed in PBS and negatively stained with 2% uranyl acetate for 5 min at room temperature. Stained grids were embedded in 2.5% methylcellulose for improved preservation and air-dried before examination.

Nucleic acid electrophoresis

The absence of genetic material in the cell membrane suspension and in the final CMVs was assessed by 1% w/v agarose gel electrophoresis in TBE buffer. The membrane pellet isolated as described above was hydrated with the appropriate volume of starting buffer, vortexed and sonicated until suspended, then mixed with 6X MassRuler DNA Loading Dye (Thermo Fisher Scientific). To verify the absence of nucleic acids inside the final CMVs undergone the complete preparation procedure, an aliquot of CMVs was disrupted by ultrasounds, before mixing with 6X MassRuler DNA Loading Dye (Sigma). Electrophoresis was run at 80 V for 30 min, with an aliquot of the parent cell homogenate as positive control.

Qualitative and quantitative protein content determination

The quantitative determination of CMV protein content was carried out, after CMV disruption by sonication (five pulses of 0.1 kJ for 10 s) using a Sonoplus Ultrasonic homogenizer (Bandelin), by spectrophotometric measurement of the UV absorbance at 280 nm. CMV protein composition was investigated, from a qualitative point of view, by proteomic analysis. Briefly, the aqueous suspension of vesicles was gently dried under a N₂ flux at room temperature; the sample was resuspended in 50 μL of iST-LYSE buffer (PreOmics) and incubated for 10 min at 95 °C on a ThermoMixer at 1000 rpm. The lysed sample was then transferred to a 96-deep well plate and

both PAC-based protein isolation on magnetic microparticles and digestion were automated on a KingFisher™ Apex magnetic handling station in a 96-well format. The magnetic beads were then removed from the digested samples and the peptide mixtures were acidified using 2% trifluoroacetic acid. The acidified sample was loaded onto a C18 column, and the peptides were analyzed on the Evosep One LC system using an EASY spray column (150 $\mu\text{m} \times 15 \text{ cm}$, Thermo Fisher Scientific) with a flow rate of 500 nL/min, at a column temperature of 40 °C. The column interfaced online with the Orbitrap Exploris 480 mass spectrometer, and mass spectrometry analysis was performed in data-independent acquisition mode.

The presence of annexin A2, identified by the proteomic analysis, on the CMV membrane was confirmed by immunofluorescence, incubating CM-DiI-labelled CMVs with an Alexa Fluor 488 anti-annexin A2 antibody at 4 °C overnight. Unbound antibodies were removed by ultracentrifugation: the mixture suspension was centrifuged at 25,000g and 4 °C for 20 min, the supernatant was discarded, and the pellet washed twice with PBS, repeating the centrifugation under the same conditions. Finally, the pellet was resuspended in PBS and observed under confocal microscope.

BSH loading evaluation

BSH loading was quantified by ICP-OES using an iCAP™ 7000 Series (Thermo Fisher Scientific) with axial plasma view for better sensitivity. Briefly, 200 μL of BSH-loaded CMVs were transferred in Teflon PFA vessels and dried under N_2 flux at 70 °C, then 3 mL of methanol were added and dried under N_2 flux; finally, 16 μL of yttrium, used as internal standard, and 3 mL of HNO_3 65% m/m (‘for trace analysis’, Scharlau Chemie) were added. Sample digestion was conducted in the closed vessels placed on a heating block at 160 °C for 6 h, then, after cooling, the solutions were diluted to 10 mL with Type I water ($> 18 \text{ M}\Omega \text{ cm}$) (Purarity TU3+, VWR International) and analyzed. BSH was quantified against a five-point calibration curve prepared by using a boron aqueous standard solution (linearity range from 0 to 10 $\mu\text{g/mL}$, corresponding to 100 μg of boron). The measurements were performed at three wavelengths (249.773 nm, 249.678 and 182.641 nm), selected to achieve high sensitivity and minimum interferences, using the Element Finder plug-in of Qtegra Intelligent Scientific Data Solution Software 2.7 (Thermo Fisher Scientific).

Encapsulation efficiency (EE%) was determined as the % ratio of the amount of BSH found in CMVs and the initial amount of BSH used, while drug loading was expressed in two different ways: as $\mu\text{g BSH}/\mu\text{g proteins}$, determined through the UV absorbance at 280 nm, and as $\mu\text{g BSH}/\text{number of CMVs}$, determined by NTA.

Stability studies

Stability of BSH-loaded CMVs was evaluated by monitoring the size and zeta potential of the vesicles over two-week storage at a temperature of 4 °C. Moreover, BSH leakage was evaluated. In particular, BSH-loaded CMVs were stored at 4 °C in a Float-A-Lyzer™ G2 dialysis device (MWCO: 500–1000 D) and after 48 h the BSH leaked from the CMVs, as well as the BSH retained inside the vesicles, was quantified by ICP-OES, following the method previously described in section “[BSH loading evaluation](#)”.

The stability of the BSH-loaded CMVs in serum was also investigated. To this aim, BSH-loaded CMVs were incubated with fetal bovine serum (FBS) in a 1:5 volume ratio at 37 °C under gentle stirring for 12 and 48 h. After filtration using 100 kDa MWCO Amicon Ultra centrifugal filters, the BSH retained inside the CMVs was quantified by ICP-OES.

Confocal imaging

A Stellaris8 Falcon TauSTED (Leica Microsystems), operating as confocal microscope, was used for fluorescence measurements. The desired excitation wavelengths were chosen using a supercontinuum white light laser ($\lambda_{\text{ex}} = 488 \text{ nm}$ for CellMask™ and Alexa Fluor 488, and $\lambda_{\text{ex}} = 561 \text{ nm}$ for CM-DiI), setting a notch filter at 488 nm and 561 nm, respectively. Two HyDS detectors (Leica Microsystems) were used to measure CellMask™/Alexa Fluor 488 and CM-DiI fluorescence emissions, in the 500–540 nm and 570–720 nm ranges, respectively, observing the samples through a plan-apochromatic oil immersion objective 100X/1.40 NA.

To assess the presence of annexin A2 on the CMV membrane, confocal imaging was performed to investigate the co-localization of the fluorescence signal of CM-DiI-labelled CMVs and Alexa Fluor 488-labeled anti-annexin A2 antibody.

For CMV internalization measurements, Z-stacks of images (1024 \times 1024 \times 16 bit) were obtained using a Z-step size of 0.7 μm and a scan speed of 600 Hz. The acquired Z-stacks were analyzed using Leica Application Suite X (LAS X) software. The time of measurement was kept below 2 h for each sample.

Unloaded and BSH-loaded CMV cellular internalization was studied by confocal microscopy. Cells (1.5×10^4) were plated on Matrigel™-coated μ -Dish 35 mm glass bottom microscopy dishes (Ibidi) and after 24 h were stained with CellMask™ Green Plasma Membrane Stain (incubation for 15 min at 37 °C). Then the cell culture medium was replaced with 1.3 mL of CM-DiI-labeled unloaded or BSH-loaded CMV suspension in PBS (approx. 6.1×10^9 particles/mL), or with 1.3 mL of CM-DiI labeled-liposomes (composed of DSPC, cholesterol and DSPE-PEG 52:45:3 mol%) suspended in PBS, as a control, incubating for 15 and 30 min at 37 °C and 5% CO_2 . CMV internalization was investigated on both parent (GBM1) and non-parent (GBM2) cancer cells, and on healthy oligodendrocytes.

BSH cell internalization was also quantified: GBM1 cells previously incubated with BSH-loaded CMVs underwent the digestion procedure, followed by ICP-OES analysis, already described in section “[BSH loading evaluation](#)”.

Flow cytometry

Cells (2.5×10^5) were grown in complete medium in 60 mm Petri dishes and incubated with 20 μL of CM-DiI-labeled CMVs for different times. Then, the cells were collected by TryPLE and the viable ones were counted by Trypan Blue dye exclusion. A minimum of 1.0×10^4 cells per sample were acquired using CytoFLEX S Flow Cytometer (Beckman Coulter) and data were processed using Kaluza software (Beckman Coulter), by standard gating to eliminate aggregates and dead cells. Untreated cells were used as reference standard.

In vitro toxicity

The reduction of MTT reagent (3-(4,5-dimethylthiazol-2-yl)-2,5-diphenyl-2H-tetrazolium bromide, Sigma-Aldrich) was used to test the cytocompatibility of unloaded CMVs with oligodendrocyte cell line and both parent (GBM1) and non-parent GBM cells, i.e. cells isolated from postsurgical specimens deriving from different patients (GBM2). The cells were plated in 96-well plates at the concentration of 3×10^3 cells/well and treated with CMVs at two different concentrations for 24 and 48 h in time-course experiments. After treatment, MTT (2.5 mg/mL in PBS) was added and incubated for 2 h at 37 °C in a 5% CO₂ environment. The water-insoluble formazan produced by MTT was solubilized with DMSO and measured through a BioTek ELx800 microplate reader in terms of its optical density (OD) at 570 nm wavelength³². The results are calculated as the % viability in relation to the control untreated cells.

Statistical analysis

The results of all experiments, repeated at least three times, were expressed as mean \pm S.D./S.E.M. Statistical analysis was carried out using Prism 5.02 (GraphPad). Statistical significance among groups was assessed by t-test one-way ANOVA followed by *post-hoc* Dunnett's test.

Results and discussion

Cell-derived biomimetic vesicles may inherit functions of the source cells, thus the choice of the appropriate type of originating cells is relevant. Indeed, the most used membrane sources for cancer cell membrane-derived nanovesicles are murine or human cancer cell lines, which ensure indefinite growth in vitro, providing an unlimited source of biological material. Nevertheless, established cancer cell lines greatly differ from clinical cancer patients and present important limitations, such as genetic aberrations accumulated with repeated in vitro passages, while primary cancer cell cultures, although having a finite period of culture, exhibit genomic and phenotypic stability, and preserve the stem-like phenotype of cancer cells, a valuable feature for preclinical studies^{33–35}. Thus, as membrane sources, we decided to use patient-derived GBM cell cultures enriched in stem-like cells. In fact, since these cells are at the basis of GBM development, progression, and therapeutic failure, to derive CMVs from this population increases the possibility to target them with high efficiency. Moreover, nowadays it is possible to grow these primary stem-like cells for long time using procedures (i.e. growth factor-containing serum free media and Matrigel™ as adhesion surface) that guarantee to preserve the original cell phenotype and biological features.

GBM cell homogenate underwent a differential centrifugation procedure to isolate the plasma membrane fraction and remove cytosolic components. The plasma membrane isolation protocol was designed adapting the procedure described by Suski et al.³⁶. Nuclei and unbroken cells were removed as pellet by the initial low-speed centrifugation (800g), while high-speed ones (10,000 and 25000g) were conducted to isolate cell membranes from the mitochondrial fraction and from cytosol components and microsomes respectively.

The purified membrane fragments were resuspended in aqueous medium and extruded through polycarbonate filters of decreasing pore size to obtain a homogeneous nanovesicle population. DLS measurements revealed monodispersed vesicles with a diameter of 121.3 ± 0.4 nm and low PDI (0.09 ± 0.01); the zeta potential was -26 ± 4 mV (Fig. 1). The fluorescent labeling with CM-DiI, performed for confocal imaging and FACS analysis, did not significantly change CMV size, PDI and zeta potential. The determination of CMV concentration by NTA (Fig. 1), resulting approximately 10^{11} particles/mL, is an important point in the characterization of a nanosystem conceived for therapeutic applications, since this parameter assures compliance to present and future regulation, like EC Recommendation for the definition of a nanomaterial (2011/696/EU)³⁷, and allows to implement effective quality assurance and quality control protocols³⁸.

TEM micrographs allowed to appreciate the spherical morphology of the CMVs (Fig. 2A), while agarose gel electrophoresis confirmed that the preparation procedure led to the isolation of a pure membrane pellet, without contamination of nucleic acids, as shown in Fig. 2B. This excludes that CMVs can carry potentially carcinogenic genetic material.

The protein content of CMV suspension was estimated as 18 $\mu\text{g/mL}$, and proteomic analysis confirmed that CMVs retained membrane proteins typical of the parent cells, as reported in Table 1. The preservation of membrane proteins on the CMV surface might be fundamental in the selective interaction of these vesicles with GBM cells.

Several of the identified membrane proteins have been reported in the literature as characteristic of GBM cells, including annexin A2³⁹, CD44⁴⁰, HLA class I histocompatibility antigen A⁴¹ and adipocyte plasma membrane-associated protein⁴². In particular, the most abundant membrane protein found in the CMVs was annexin A2, a calcium-binding protein expressed on the surface of macrophages, mononuclear and endothelial cells, as well as in several types of cancer cells⁴³. The expression of annexin A2 has been associated with cell dissemination and metastasis in many cancer types; it is overexpressed in GBM cells and positively correlated with tumor aggressiveness and progression sustaining cell invasion, angiogenesis, proliferation, matrix invasion and mesenchymal transition^{44,45}. Interestingly, knockdown of annexin A2 decreased glioma cell migration in vitro and slowed down tumor progression in vivo, as evidenced by decreased proliferation, invasion, and angiogenesis⁴⁶.

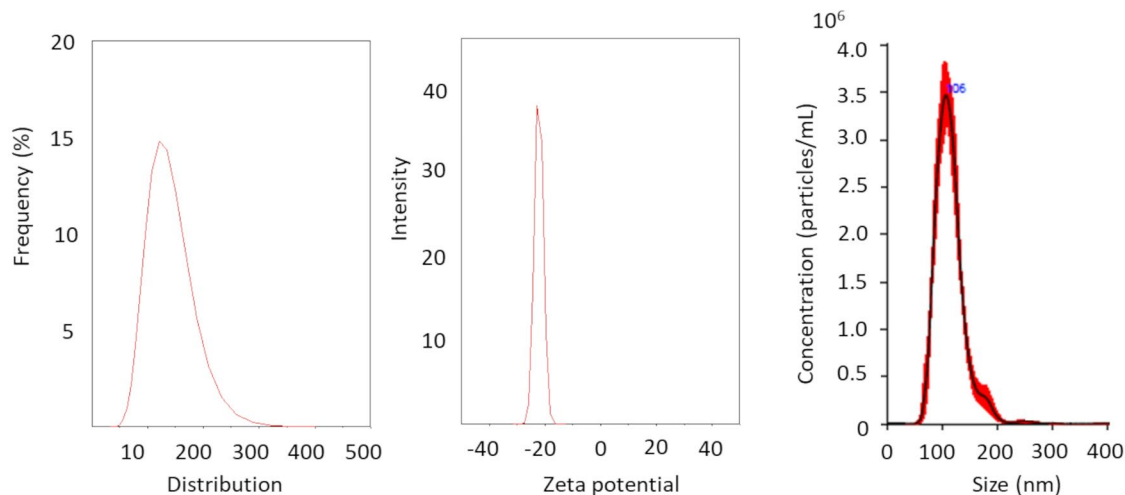


Figure 1. On the left: CMV size distribution by intensity; in the middle: CMV zeta potential; on the right: CMV concentration vs size distribution measured by NTA (sample dilution 1:500).

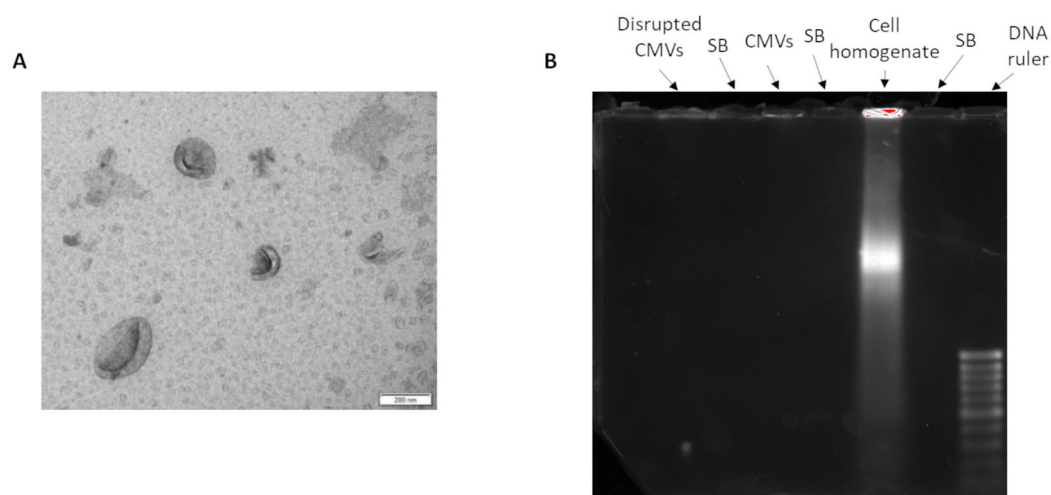


Figure 2. (A) TEM micrograph of the CMVs, magnification bar = 200 nm; (B) Agarose gel electrophoresis revealing the absence of genetic material in CMVs, even when disrupted by ultrasonication. A slight overexposure was applied to the gel to further validate the absence of genetic material in the CMV samples.

To further investigate the presence of annexin A2 on the surface of the CMVs, the vesicles were incubated with a fluorescent labelled anti-annexin antibody and, after removal of the unbound ligands, a drop of suspension was observed through confocal microscopy. As shown in Fig. 3, a co-localization of the red fluorescent signal, deriving from the CM-DiI-labeled CMVs, and of the green fluorescent signal deriving from the Alexa Fluor 488-labeled anti-annexin antibody, was highlighted.

Many strategies for the loading of exosomes and extracellular vesicles with small molecules are reported in the literature⁴⁷, with sonication and electroporation being the most promising. Therefore, to load BSH into CMVs, we investigated both techniques. The EE% and drug loading values obtained from the two loading procedures are reported in Table 2. The electroporation method gave more rewarding results, with a consistent amount of BSH encapsulated, also if compared to the results reported by other authors⁴⁸.

Noteworthy, in most literature works reporting the loading of exosomes and other biomimetic nanosystems with active molecules, drug loading is expressed as amount of drug/amount of proteins; however, we decided to express it also in terms of μg BSH/number of CMVs, which might be more informative in the case of clinical application.

Since both loading procedures might impair vesicle integrity, the mean size and PDI of CMVs was monitored after the loading and purification processes. As shown in Fig. 4, the sonication procedure did not significantly affect the mean size and PDI; on the contrary, the electroporation procedure led to a significant increase in CMV mean size (from 125 ± 2 nm to 176 ± 3 nm), accompanied by a PDI increase (from 0.1 ± 0.1 to 0.4 ± 0.2), possibly due to a little extent of aggregation phenomena caused by the electric field⁴⁹. However, even if significantly

Protein group	Protein name	Protein gene	Amount (Log2)
P07355	Annexin A2	ANXA2	12.10
P26006	Integrin alpha-3	ITGA3	11.75
F8VNT9; F8VV56; F8VWK8; F8W022; P08962; P08962-2; P08962-3	CD63 antigen	CD63	11.49
H0YD13; P16070; P16070-10; P16070-11; P16070-12; P16070-13; P16070-14; P16070-16; P16070-17; P16070-18; P16070-3; P16070-4; P16070-5; P16070-6; P16070-7; P16070-8	CD44 antigen	CD44	11.46
A0A7P0TA85; P35613; P35613-2	Basigin	BSG	11.45
A0A7I2V2F9; E7EUI6; H7C4K3; P05556	Integrin beta	ITGB1	11.21
P21589	5'-nucleotidase	NT5E	11.09
A0A1W2PS24; P04439; Q5SRN5; Q5SRN7	HLA class I histocompatibility antigen, A alpha chain	HLA-A	10.76
P13473-2	Isoform LAMP-2B of Lysosome-associated membrane glycoprotein 2	LAMP2	10.50
A0A2U3TZL5; E9PNW4; P13987; P13987-2	CD59 glycoprotein	CD59	10.50
P54709	Sodium/potassium-transporting ATPase subunit beta-3	ATP1B3	10.48
A0A2R8Y484; Q08722; Q08722-2; Q08722-3; Q08722-4	Leukocyte surface antigen CD47	CD47	10.11
O43570; O43570-2	Carbonic anhydrase 12	CA12	9.83
Q9HDC9	Adipocyte plasma membrane-associated protein	APMAP	9.36

Table 1. Most abundant membrane proteins found with the proteomic analysis of a CMV sample.

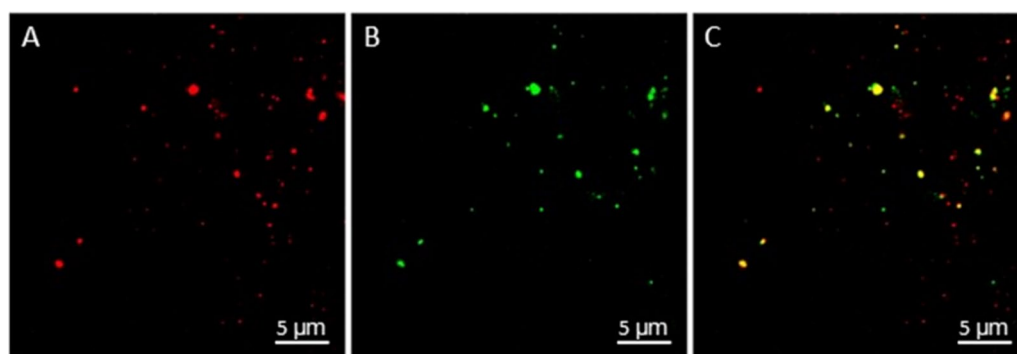


Figure 3. Confocal images of CM-DiI-labeled CMVs after incubation with anti-annexin A2 antibody labeled with the Alexa Fluor 488 dye. (A) Red fluorescent signal deriving from CM-DiI-labelled CMVs ($\lambda_{\text{ex}} = 561 \text{ nm}$); (B) Green fluorescent signal deriving from the Alexa Fluor 488-labelled anti-annexin A2 antibody ($\lambda_{\text{ex}} = 488 \text{ nm}$); (C) Merged image, highlighting the co-localization of the two dyes.

Loading method	EE%	Drug loading ($\mu\text{g BSH}/\mu\text{g proteins}$)	Drug loading ($\mu\text{g BSH}/10^{10} \text{ CMVs}$)
Sonication	0.17 ± 0.02	3.7 ± 0.1	24 ± 2
Electroporation	2.10 ± 0.08	45.4 ± 1.9	295 ± 12

Table 2. EE% and drug loading results obtained from the two different loading procedures. Results are expressed as mean \pm standard deviation ($n = 3$).

enlarged, the CMVs subjected to electroporation maintained their nanosized dimensions, acceptable for parental administration, and the PDI value is still indicating the presence of a monodisperse population.

The size and zeta potential of BSH-loaded CMVs did not significantly change ($p < 0.05$) over two-week storage at 4°C , confirming the stability of the system at the storage conditions during this timeframe (Figs. 5A,B).

BSH leakage, as well as BSH retained inside the CMVs, was evaluated over 48 h storage at 4°C . The boron amount found outside the vesicles, measured by ICP-OES, was below the limit of detection of the method. Contrarily, as shown in Fig. 5C, the boron found inside the CMVs confirmed a consistent retainment of BSH even after two-week storage.

BSH-loaded CMVs exhibited good stability even when incubated with FBS at 37°C . Indeed, ICP-OES analysis evidenced that 43.4 ± 2.0 and $44.8 \pm 1.7 \mu\text{g BSH}/\mu\text{g proteins}$ were found inside the CMVs after 12 and 48 h incubation in FBS, respectively, values not significantly different from the drug loading value already reported in Table 2 ($p < 0.05$). These promising preliminary results should be further investigated, and this kind of test should

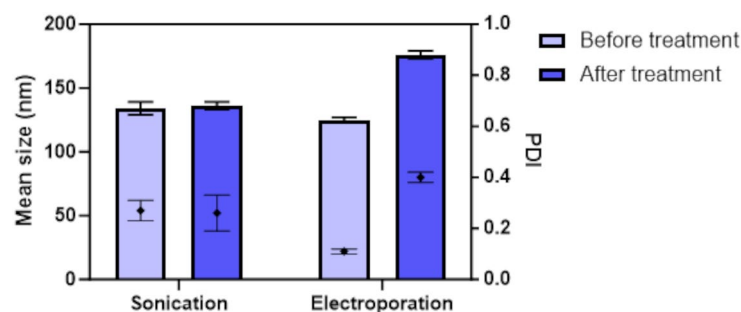


Figure 4. Mean CMV size and PDI values before and after BSH loading, carried out by sonication and electroporation. Mean \pm standard deviation ($n = 3$).

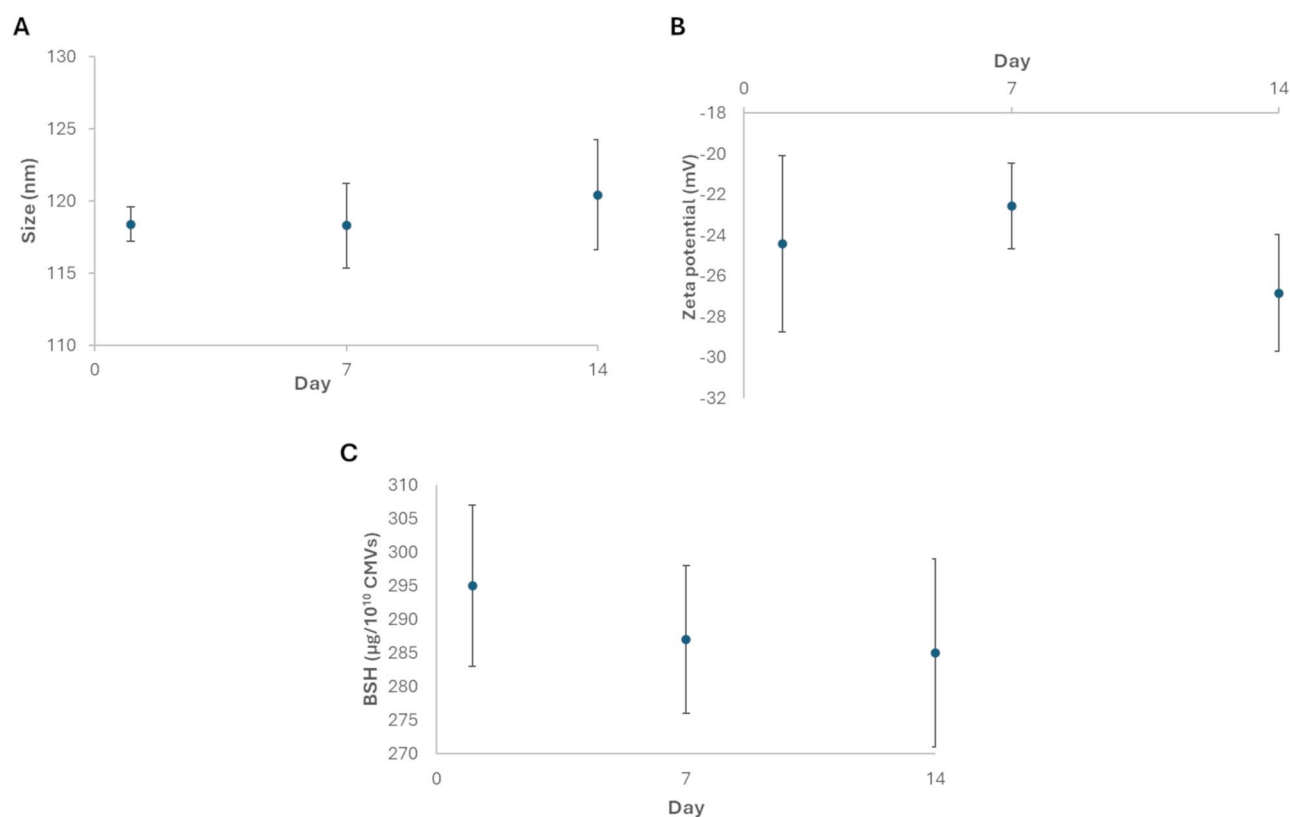


Figure 5. Stability of the BSH-loaded CMVs over 2 week storage at 4 °C, monitoring the size (A), zeta potential (B) and BSH content (C).

also be performed using human serum, to further validate the BSH-loaded CMVs suitability for i.v. injection, even if other routes of administration might be considered (i.e., local administration).

The cell-specific targeting ability of the CMVs was demonstrated by *in vitro* internalization studies. As shown in Fig. 6, CMV association with both parent (GBM1) and non-parent (GBM2) cell membranes was clearly evident as soon as after 15 min incubation (Fig. 5A,C), while the interaction with human oligodendrocytes was negligible (Fig. 5E). After 30 min incubation, the amount of internalized CMVs significantly increased in both GBM1 and GBM2 cells (Fig. 5B,D), while the interaction with healthy oligodendrocytes remained limited (Fig. 5F). Conversely, artificial liposomes were able to barely interact with GBM1 cells at both incubation times, excluding that CMV binding to cell membranes and internalization were due to non-specific interaction of phospholipids with cell membrane proteins and lipids (Fig. 5G,H). This corroborates the concept of using cell membrane fragments for formulating delivery vesicles, naturally bearing targeting molecules that would be difficult to attach to an artificial liposome surface. Moreover, the low interaction of CMVs with normal oligodendrocytes suggested that CMV internalization involves specific membrane proteins expressed in GBM cells, but not in healthy cells.

As shown in Fig. 7, BSH-loaded CMVs showed consistent interaction with GBM1 cells, confirming that the encapsulation of the boronated agent did not influence the interaction of the CMVs with the target cells. Moreover, GBM1 cells incubated with BSH-loaded CMVs revealed a boron content equivalent to about 6×10^{11} B atoms/

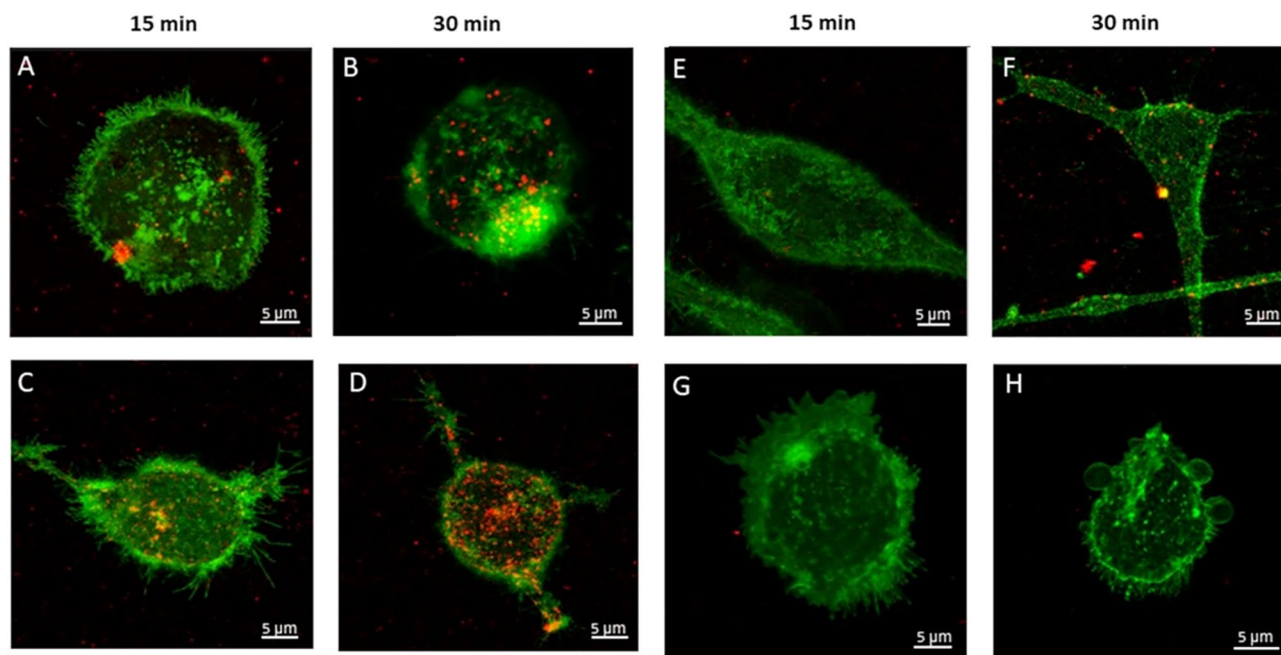


Figure 6. Confocal images obtained by the superimposition of different cell stacks (0.7 μm height). CM-DiI-labeled CMVs (red) incubated for 15 and 30 min with the green fluorescent parent GBM1 cells (A and B), non-parent GBM2 cells (C and D), and human M03.13 oligodendrocytes (E and F). CM-DiI-labeled liposomes were also incubated with GBM1 cells (G and H), to rule out a non-specific interaction of phospholipids with GBM cells. Scale bar 5 μm .

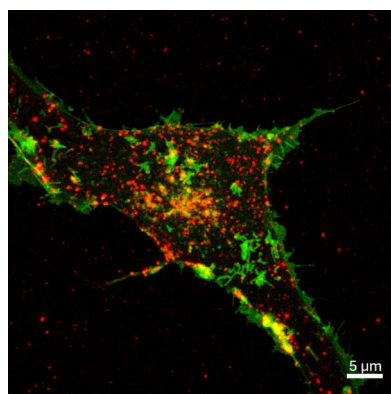


Figure 7. Confocal image obtained by the superimposition of different cell stacks (0.7 μm height). CM-DiI-labeled and BSH-loaded CMVs (red) incubated for 30 min with the green fluorescent parent GBM1 cells.

cell. Considering that, for effective BNCT, 10^9 atoms/cell have to be selectively delivered to the tumor, this is a very promising result, even if *in vivo* studies are obviously necessary to confirm that the BSH-loaded CMVs are able to selectively deliver to the tumor tissue a sufficient amount of boron to exert a cytotoxic effect, upon neutron irradiation.

Flow cytometry confirmed the time-dependent interaction of the GBM1-derived CM-DiI-labelled CMVs with both parent and non-parent GBM cells in a more quantitative way. Indeed, while after 30 min incubation only 2.5% of parent cells (GBM1) were positive to the fluorescent emission associated to CM-DiI-CMVs, this value increased to 76.9% and 81.2% after 16- and 24 h incubation, respectively (Fig. 8). The analysis performed on non-parent GBM2 cells confirmed the high degree of uptake already observed through confocal microscopy, and the heterologous tropism of GBM-derived CMVs for GBM cells (Fig. 8F).

Since the absence of toxicity of BSH without neutron irradiation is already documented by the numerous clinical trials and works in the literature²², the absence of non-specific toxicity caused by empty CMVs cell internalization was investigated. The MTT assay revealed negligible (< 20% after 48 h incubation with the highest concentration tested), time-independent toxicity of the CMVs on oligodendrocytes, as shown in Fig. 9A. As compared to human oligodendrocyte cultures, CMVs exerted slightly higher toxicity on GBM cells, both parent and non-parent ones, showing a time-dependent effect; this might be explained by considering the wide

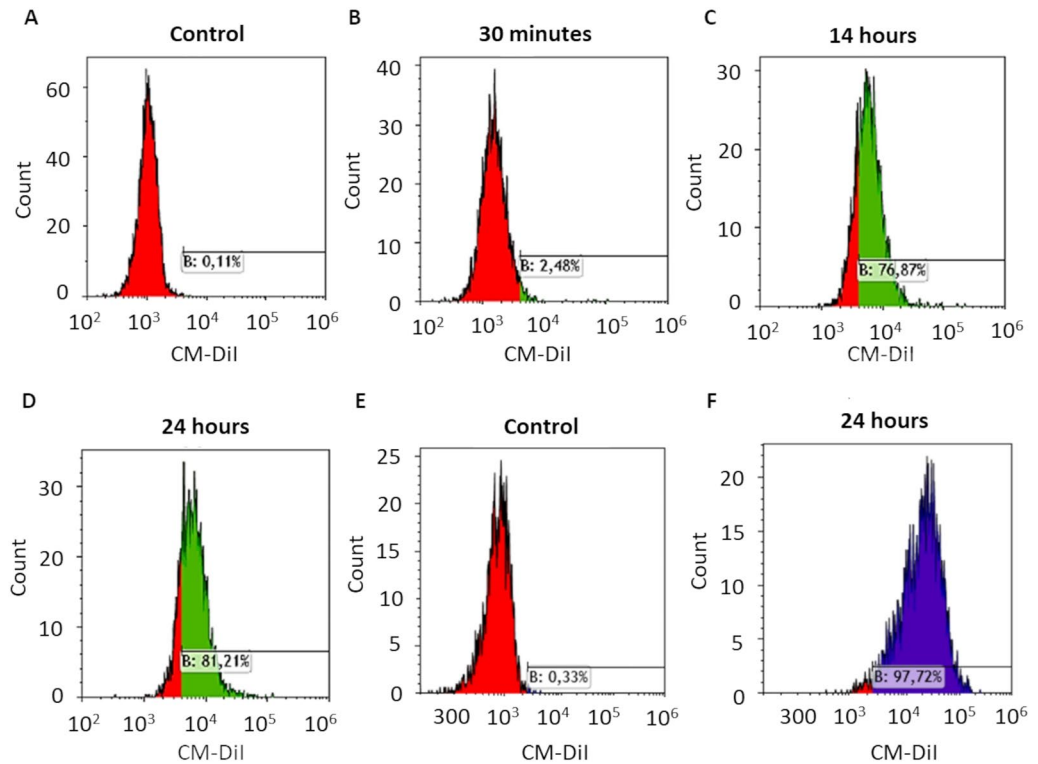


Figure 8. Flow cytometry histograms representing relative CM-DiI fluorescence intensity (x-axis) and the number of events (count, y-axis). Parent GBM1 cells not incubated with CM-DiI labeled CMVs (A), incubated with CM-DiI-labeled CMVs for 30 min (B), with CM-DiI-labeled CMVs for 16 h (C) and with CM-DiI-labeled CMVs for 24 h (D); non-parent GBM2 cells not incubated with CM-DiI labeled CMVs (E), and incubated with CM-DiI-labeled CMVs for 24 h (F).

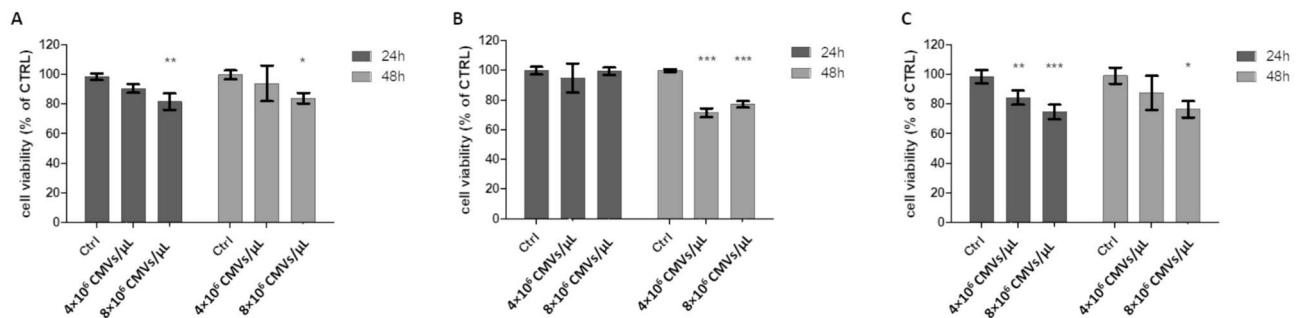


Figure 9. Cell viability in control and CMV-treated cells assessed by MTT assay on human M03.13 oligodendrocyte cell line (A), parent GBM1 cells (B) and non-parent GBM2 cells (C). Two different CMVs concentrations and two time points were tested. * $p < 0.05$; ** $p < 0.01$; *** $p < 0.001$ versus control.

differences existing between oligodendrocytes and GBM cells, in terms of proliferation rate and cellular metabolism. Moreover, the higher internalization of CMVs into GBM cells, leading during time to a high number of internalized vesicles, might further explain this cytotoxic effect observed.

Conclusions

In this study we set up a procedure to prepare nanovesicles composed of GBM cell membranes, following an optimized isolation protocol to eliminate any potentially detrimental genetic material. The obtained CMVs have been thoroughly characterized for their physical–chemical properties, including the vesicle concentration in suspension, which is a key aspect in the characterization of a nanosystem conceived for the delivery of therapeutic agents. Importantly, we were able to demonstrate that GBM-derived CMVs display a specific tropism toward GBM stem-like cells, being internalized by these cells and able to release high boron levels inside their cytosol, while low internalization occurred in a cell line model of normal oligodendrocytes. Proteomic analysis allows

the identification of specific membrane proteins that characterize the parent cells from which the membrane material was isolated, likely mediating the internalization observed in vitro.

BSH, a promising BNCT agent already used in clinical trials, was loaded into the vesicles by following two different procedures, being the electroporation the most efficient in terms of drug loading, clearly supporting the possibility to use this cell membrane vesicular system as potential drug carrier towards in vivo tumors. Noteworthy, the high internalization rate obtained in the GBM stem-like cells isolated from different patients widens the versatility of this drug delivery system not only to the treatment of the patient from which the source cells were isolated, paving the way for a broader application. The low interaction with normal cells may cause a high selectivity of the drug delivery toward tumor cells reducing the toxicity for normal brain cells, which represent a major limitation in the treatment of gliomas. Moreover, the possibility to target glioma stem cells, which are nowadays considered the real target for all the antitumoral therapies, represents a further added value at the therapeutic potential of the nanovesicular system we describe in this study.

Data availability

The datasets generated during and/or analyzed during the current study are available from the corresponding authors on reasonable request.

Received: 10 April 2024; Accepted: 6 August 2024

Published online: 20 August 2024

References

1. Maher, E. A. *et al.* Malignant glioma: Genetics and biology of a grave matter. *Genes Dev.* **15**, 1311–1333 (2001).
2. Florio, T. & Barbieri, F. The status of the art of human malignant glioma management: The promising role of targeting tumor-initiating cells. *Drug Discov. Today* **17**, 1103–1110 (2012).
3. Ostrom, Q. T. *et al.* The epidemiology of glioma in adults: A 'state of the science' review. *Neuro-Oncology* **16**, 896–913 (2014).
4. Grochans, S. *et al.* Epidemiology of glioblastoma multiforme-literature review. *Cancers* **14**, 2412 (2022).
5. Furnari, F. B. *et al.* Malignant astrocytic glioma: Genetics, biology, and paths to treatment. *Genes Dev.* **21**, 2683–2710 (2007).
6. Omuro, A. & DeAngelis, L. M. Glioblastoma and other malignant gliomas: A clinical review. *JAMA* **310**, 1842–1850 (2013).
7. Stupp, R. *et al.* Radiotherapy plus concomitant and adjuvant temozolomide for glioblastoma. *N. Engl. J. Med.* **352**, 987–996 (2005).
8. Gouazé-Andersson, V. & Cohen-Jonathan Moyal, E. New avenues in radiotherapy of glioblastoma: From bench to bedside. *Curr. Treat. Options Neurol.* **22**, 45 (2020).
9. Ailuno, G., Baldassari, S., Lai, F., Florio, T. & Caviglioli, G. Exosomes and extracellular vesicles as emerging theranostic platforms in cancer research. *Cells* **9**, 2569 (2020).
10. Wu, J.-Y. *et al.* Exosomes and biomimetic nanovesicles-mediated anti-glioblastoma therapy: A head-to-head comparison. *J. Control. Release* **336**, 510–521 (2021).
11. Oieni, J. *et al.* Nano-Ghosts: Biomimetic membranal vesicles, technology and characterization. *Methods Extracell. Vesicles Mimetics* **177**, 126–134 (2020).
12. Toledano Furman, N. E. *et al.* Reconstructed stem cell nanoghosts: A natural tumor targeting platform. *Nano Lett.* **13**, 3248–3255 (2013).
13. Liu, X., Zhong, X. & Li, C. Challenges in cell membrane-camouflaged drug delivery systems: Development strategies and future prospects. *Chin. Chem. Lett.* **32**, 2347–2358 (2021).
14. Ren, Y. *et al.* Homotypic cancer cell membranes camouflaged nanoparticles for targeting drug delivery and enhanced chemophotothermal therapy of glioma. *Pharmaceuticals* **15**, 157 (2022).
15. Rayamajhi, S., Nguyen, T. D. T., Marasini, R. & Aryal, S. Macrophage-derived exosome-mimetic hybrid vesicles for tumor targeted drug delivery. *Acta Biomater.* **94**, 482–494 (2019).
16. Hu, K. *et al.* Boron agents for neutron capture therapy. *Coord. Chem. Rev.* **405**, 213139 (2020).
17. Barth, R. F. *et al.* Current status of boron neutron capture therapy of high grade gliomas and recurrent head and neck cancer. *Radiat. Oncol.* **7**, 146 (2012).
18. Miyatake, S.-I. *et al.* Boron neutron capture therapy of malignant gliomas. *Prog. Neurol. Surg.* **32**, 48–56 (2018).
19. Hiratsuka, J. *et al.* Boron neutron capture therapy for vulvar melanoma and genital extramammary Paget's disease with curative responses. *Cancer Commun.* **38**, 38 (2018).
20. Matsuya, Y., Fukunaga, H., Omura, M. & Date, H. A model for estimating dose-rate effects on cell-killing of human melanoma after boron neutron capture therapy. *Cells* **9**, 1117 (2020).
21. Barth, R. F., Mi, P. & Yang, W. Boron delivery agents for neutron capture therapy of cancer. *Cancer Commun.* **38**, 35 (2018).
22. Ailuno, G. *et al.* Boron vehiculating nanosystems for neutron capture therapy in cancer treatment. *Cells* **11**, 4029 (2022).
23. Wu, J.-Y. *et al.* Multifunctional exosome-mimetics for targeted anti-glioblastoma therapy by manipulating protein corona. *J. Nanobiotechnol.* **19**, 405 (2021).
24. Jia, Y. *et al.* Phototheranostics: Active targeting of orthotopic glioma using biomimetic proteolipid nanoparticles. *ACS Nano* **13**, 386–398 (2019).
25. Guo, Y. *et al.* Eliminating the original cargos of glioblastoma cell-derived small extracellular vesicles for efficient drug delivery to glioblastoma with improved biosafety. *Bioact. Mater.* **16**, 204–217 (2022).
26. Lu, G. *et al.* Engineered biomimetic nanoparticles achieve targeted delivery and efficient metabolism-based synergistic therapy against glioblastoma. *Nat. Commun.* **13**, 4214 (2022).
27. Chen, H. *et al.* Biomimetic nanosonosensitizers combined with noninvasive ultrasound actuation to reverse drug resistance and sonodynamic-enhanced chemotherapy against orthotopic glioblastoma. *ACS Nano* **17**, 421–436 (2023).
28. Barbieri, F. *et al.* Chloride intracellular channel 1 activity is not required for glioblastoma development but its inhibition dictates glioma stem cell responsiveness to novel biguanide derivatives. *J. Exp. Clin. Cancer Res. CR* **41**, 53 (2022).
29. Barbieri, F. *et al.* Inhibition of chloride intracellular channel 1 (CLIC1) as biguanide class-effect to impair human glioblastoma stem cell viability. *Front. Pharmacol.* **9**, 899 (2018).
30. Griffero, F. *et al.* Different response of human glioma tumor-initiating cells to epidermal growth factor receptor kinase inhibitors*. *J. Biol. Chem.* **284**, 7138–7148 (2009).
31. Yerneni, S. S. *et al.* Skin-targeted delivery of extracellular vesicle-encapsulated curcumin using dissolvable microneedle arrays. *Acta Biomater.* **149**, 198–212 (2022).
32. Bajetto, A. *et al.* different effects of human umbilical cord mesenchymal stem cells on glioblastoma stem cells by direct cell interaction or via released soluble factors. *Front. Cell. Neurosci.* **11**, 312 (2017).
33. Barbieri, F. *et al.* Stem-like signatures in human meningioma cells are under the control of CXCL11/CXCL12 chemokine activity. *Neuro-Oncology* **25**, 1775–1787 (2023).

34. Richter, M. *et al.* From donor to the lab: A fascinating journey of primary cell lines. *Front. Cell Dev. Biol.* **9**, 711381 (2021).
35. Würth, R. *et al.* Phenotypical and pharmacological characterization of stem-like cells in human pituitary adenomas. *Mol. Neurobiol.* **54**, 4879–4895 (2017).
36. Suski, J. M. *et al.* Isolation of plasma membrane-associated membranes from rat liver. *Nat. Protoc.* **9**, 312–322 (2014).
37. Austin, J., Minelli, C., Hamilton, D., Wywijas, M. & Jones, H. J. Nanoparticle number concentration measurements by multi-angle dynamic light scattering. *J. Nanoparticle Res.* **22**, 108 (2020).
38. Ailuno, G. *et al.* Development of biotinylated liposomes encapsulating metformin for therapeutic targeting of inflammation-based diseases. *Pharmaceutics* **16**, 235 (2024).
39. Sharma, M. C. Annexin A2 (ANX A2): An emerging biomarker and potential therapeutic target for aggressive cancers. *Int. J. Cancer* **144**, 2074–2081 (2019).
40. Lubanska, D. *et al.* Impairing proliferation of glioblastoma multiforme with CD44+ selective conjugated polymer nanoparticles. *Sci. Rep.* **12**, 12078 (2022).
41. Rose, M. *et al.* Surfaceome proteomic of glioblastoma revealed potential targets for immunotherapy. *Front. Immunol.* **12**, 746168 (2021).
42. Mallawaarachy, D. M. *et al.* Membrane proteome analysis of glioblastoma cell invasion. *J. Neuropathol. Exp. Neurol.* **74**, 425–441 (2015).
43. Hedhli, N. *et al.* The annexin A2/S100A10 system in health and disease: Emerging paradigms. *J. Biomed. Biotechnol.* **2012**, 406273 (2012).
44. Matsumoto, Y. *et al.* Annexin A2-STAT3-oncostatin M receptor axis drives phenotypic and mesenchymal changes in glioblastoma. *Acta Neuropathol. Commun.* **8**, 42 (2020).
45. Maule, F. *et al.* Annexin 2A sustains glioblastoma cell dissemination and proliferation. *Oncotarget* **7**, 54632–54649 (2016).
46. Zhai, H. *et al.* Annexin A2 promotes glioma cell invasion and tumor progression. *J. Neurosci. Off. J. Soc. Neurosci.* **31**, 14346–14360 (2011).
47. Zeng, H. *et al.* Current strategies for exosome cargo loading and targeting delivery. *Cells* **12**, 1416 (2023).
48. Hirase, S. *et al.* Dodecaborate-encapsulated extracellular vesicles with modification of cell-penetrating peptides for enhancing macropinocytotic cellular uptake and biological activity in boron neutron capture therapy. *Mol. Pharm.* **19**, 1135–1145 (2022).
49. Pomatto, M. A. C. *et al.* Improved loading of plasma-derived extracellular vesicles to encapsulate antitumor miRNAs. *Mol. Ther. Methods Clin. Dev.* **13**, 133–144 (2019).

Acknowledgements

Work supported by #NEXTGENERATIONEU (NGEU) and funded by the Ministry of University and Research (MUR), National Recovery and Resilience Plan (NRRP), project MNESYS (PE0000006)—A Multiscale integrated approach to the study of the nervous system in health and disease (DN. 1553 11.10.2022)

Author contributions

A.B. and G.A. equally contributed to this work and both should be considered as first author. T.F. and G.C. contributed equally to this work and both should be considered as last senior authors. A.B.: Conceptualization; Methodology; Investigation; Writing—Review and Editing; G.A.: Conceptualization; Methodology; Investigation; Writing—Original Draft; Writing—Review and Editing; S.B.: Methodology; Writing—Original Draft; Writing—Review and Editing; G.D.: Methodology; Investigation; Resources; Writing—Review and Editing; A.P.: Methodology; Investigation; Resources; N.G.: Investigation; O.C.: Methodology; Resources; Writing—Review and Editing; E.A.: Investigation; A.L.: Investigation; P.C.: Investigation; A.C.: Investigation; B.T.: Investigation; F.B.: Formal analysis; Investigation; Writing—Review and Editing; S.T.: Investigation; P.C.: Investigation; K.C.: Investigation; T.F.: Methodology; Resources; Writing—Review and Editing; Supervision; Funding acquisition; G.C.: Conceptualization; Methodology; Resources; Writing—Review and Editing; Supervision; Funding acquisition. All authors have read and approved the final version of the manuscript.

Competing interest

The authors declare that they have no known competing financial interests or personal relationships that could have appeared to influence the work reported in this paper.

Additional information

Correspondence and requests for materials should be addressed to G.A. or T.F.

Reprints and permissions information is available at www.nature.com/reprints.

Publisher's note Springer Nature remains neutral with regard to jurisdictional claims in published maps and institutional affiliations.

Open Access This article is licensed under a Creative Commons Attribution-NonCommercial-NoDerivatives 4.0 International License, which permits any non-commercial use, sharing, distribution and reproduction in any medium or format, as long as you give appropriate credit to the original author(s) and the source, provide a link to the Creative Commons licence, and indicate if you modified the licensed material. You do not have permission under this licence to share adapted material derived from this article or parts of it. The images or other third party material in this article are included in the article's Creative Commons licence, unless indicated otherwise in a credit line to the material. If material is not included in the article's Creative Commons licence and your intended use is not permitted by statutory regulation or exceeds the permitted use, you will need to obtain permission directly from the copyright holder. To view a copy of this licence, visit <http://creativecommons.org/licenses/by-nc-nd/4.0/>.

© The Author(s) 2024